ACS SENSORS

pubs.acs.org/acssensors

Article

Ultrasensitive Sandwich-Type SERS-Biosensor-Based Dual Plasmonic Superstructure for Detection of Tacrolimus in Patients

Xiaoyue Zheng, Jiazhou Ye, Weiwei Chen, Xiaoyuan Wang, Jianhua Li, Fengmei Su, Caiping Ding,* and Youju Huang*

Cite This: *ACS Sens.* 2022, 7, 3126−3134

Read Online

ACCESS | Metrics & More | Article Recommendations | Supporting Information

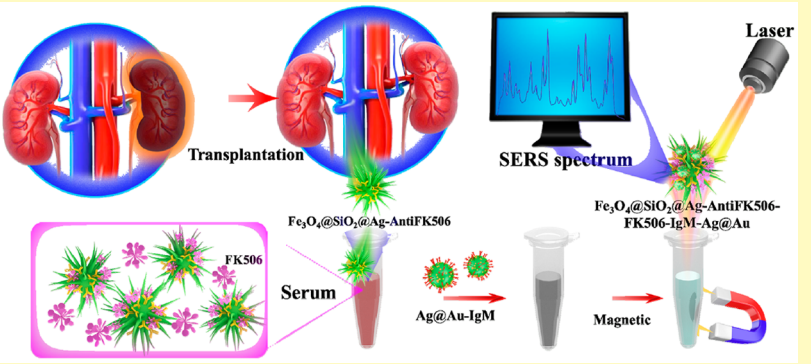

ABSTRACT: Tacrolimus (FK506) is widely used in the prevention of organ transplant rejection and the treatment of autoimmune diseases, but it is difficult to detect within the low and narrow concentration range in practical clinical fields. A magnetic plasmonic superstructure-targets-plasmonic superstructure-based sandwich-type SERS biosensor is presented here to ultrasensitively detect FK506 in the blood of organ transplant patients. The spiky Fe_3O_4@SiO_2@Ag flower magnetic superstructure and hollow Ag@Au superstructure enhanced the SERS signals by providing rich sharp tips, cavities, and abundant hot spot gaps. And the magnetic feature makes it easy to concentrate and separate the biological target. Using the designed sandwich-type SERS biosensor, FK506 could be detected within a range of 0.5−20 ng/mL with a detection limit of 0.33 ng/mL. All results indicated that the sandwich-type SERS biosensor has good stability, sensitivity, and anti-interference properties. It is noteworthy that this allowed us to successfully analyze FK506 in the blood of transplant patients, which is in strong agreement with the clinical results. Consequently, the attractive sandwich-type SERS biosensor can be used for the detection of FK506 in real samples, which is promising for clinical diagnosis.

KEYWORDS: *SERS, plasmonic superstructure, sandwich-type, FK506, clinical diagnosis*

Tacrolimus (FK506) is a commonly prescribed immunosuppressant used to prevent organ and tissue rejection in patients who have undergone a transplant. In large, prospective, randomized, multicenter trials, FK506 proved to be more effective than cyclosporine microemulsion in enhancing survival of patients and their grafts following solid organ transplantation.[1] The FK506-based maintenance immunosuppression therapy is associated with a significantly lower rate of acute rejection and better graft survival compared to the cyclosporine A-based regimen.[2] Generally, FK506 has a very narrow therapeutic window, with a concentration range of approximately 5−20 ng/mL in kidney transplant patients.[3−5] Several diseases such as chronic allograft nephropathy, diabetes mellitus, arterial hypertension, and neurotoxicity have been linked to FK506 concentrations.[6] Due to the severity of potential adverse effects, it is imperative for physicians to routinely monitor patients on an FK506-based immunosuppressive regimen.[7] Therefore, it is essential and important to develop a simple method for monitoring FK506 levels in real time in clinical settings.

FK506 has been detected in blood through a variety of methods over the past 30 years, which can primarily be grouped into three categories: immunoassays,[8−10] chromatographic methods (mainly including LC-MS/MS),[11,12] and volumetric absorption microsampling (VAMS) combined with liquid mass methods. There are some disadvantages associated with the widespread use of the immunoassay technique, particularly when certain antigens with a similar structure are present in a system, the obtained results will be influenced by

Received: July 25, 2022
Accepted: September 29, 2022
Published: October 7, 2022

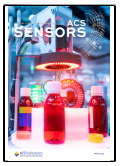

https://doi.org/10.1021/acssensors.2c01603
ACS Sens. 2022, 7, 3126−3134

Scheme 1. Schematic Preparation of Dual Plasmonic Superstructures and Sandwich-Type Sensor for Detecting FK506 in Patient Blood Samples Based on SERS

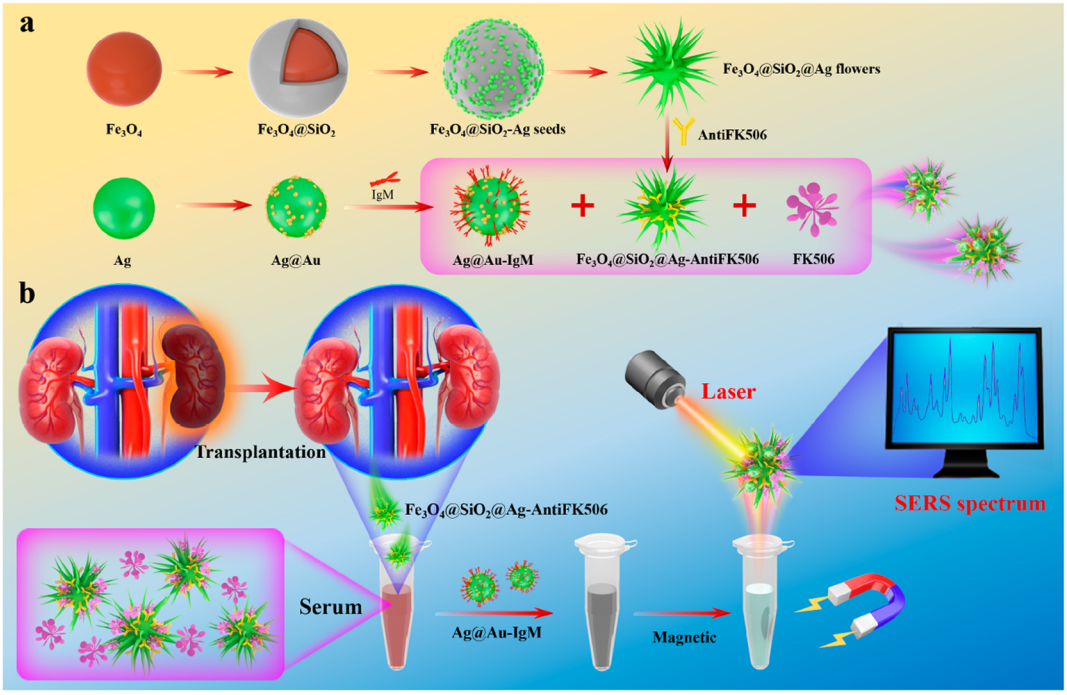

cross-reactivity. The LC-MS/MS method is easier to distinguish than the immunoassay. The LC-MS/MS methods do have some disadvantages, including a time-consuming assay, expensive instrumentation, the pretreatment, and centralization for blood samples in a qualified laboratory. VAMS technology allows for convenient, minimally invasive, and economical collection of blood from the patient's home and can even be combined with LC-MS/MS to detect the presence of FK506 in the blood. Raman spectroscopy is a new generation of detection technology that has already achieved initial results in the laboratory, which are promising in definitely providing patients with a better consultation experience in clinic use.

Surface-enhanced Raman scattering (SERS) enhances the Raman signal 10^5-fold and enables single-molecule identification.[13] Due to its ability to reveal relevant chemical, biological, material, and structural information, SERS has evolved into an interdisciplinary analysis technique with the advantages of cost-effectiveness, ultrahigh sensitivity, a narrow Raman band, multiplexing capability, and light stability.[14−20] In order to improve SERS sensitivity, rational design of substrates with different nanomaterial structures becomes important, since Raman enhancement is affected by the composition, size, and substrate with nanomaterial structures.[21] A nanostructure modified with precious metals has strong enhancement (called hot spots) in the electromagnetic field due to the plasma coupling effect in the gaps between particles.[22]

Previously, we prepared various SERS substrates with different nanomaterial structures for the construction of SERS-active biosensors.[18,23−28] A plasmonic superstructure with strong, uniform, and stable SERS "hot spot" areas was confirmed to improve SERS activity.[29−32] For example, flower-shaped nanoparticles with branched superstructures have large relative surface area and rough surface morphology for SERS enhancement.[33] And the magnetic structure has distinguished itself for rapid in vitro detection because it can be quickly separated and recovered to enrich the target for further sensitivity improvement. As the petals of a Ag flower have a strong resonance hot spot superstructure, this results in a large relative surface area for the capture of a target.[34] In addition, Au@Ag core−shell nanoparticles showed higher SERS enhancement than monometallic Au or Ag nanoparticles of similar size.[35,36] In view of the SERS enhancing mechanism and previous work,[18,23−28] we believe that the design of SERS materials should be optimized in terms of material composition, sharp tips, cavities, and hot-spots in order to maximize SERS signal amplification. Therefore, the development of the most attractive plasmonic superstructure-based biosensor will enable the detection of FK506 in real samples in an easy, fast, and sensitive manner.

Here, the plasmonic superstructure of $Fe_3O_4@SiO_2@Ag$ flowers and Ag@Au are synthesized and specifically modified with antibodies to construct a sandwich-type SERS sensor capable of rapidly and efficiently detecting FK506. As shown in Scheme 1, the highly branched petals of the magnetic plasmonic superstructure of $Fe_3O_4@SiO_2@Ag$ flowers provide a large surface area for effective capture target and generation of plasma hot spots. The miniature magnetic core gives $Fe_3O_4@SiO_2@Ag$ flowers superior magnetic properties, which further enrich the target. Next, the coupled AntiFK506 antibodies on the surfaces of $Fe_3O_4@SiO_2@Ag$ flowers show high specificity and sensitivity for the target FK506. And the antibody IgM-modified Ag@Au plasmonic superstructure is also used to target FK506, forming a plasmonic superstructure-targets-plasmonic superstructure sandwich structure ($Fe_3O_4@SiO_2@Ag$-AntiFK506-FK506-IgM-Ag@Au) to maximally amplify the SERS signals. As a result of the dual plasmonic superstructure, FK506 can be detected at concentrations ranging from 0.5 to 20 ng/mL, with a minimum detection limit of 0.33 ng/mL. Importantly, the sensor could be successfully

https://doi.org/10.1021/acssensors.2c01603
ACS Sens. 2022, 7, 3126−3134

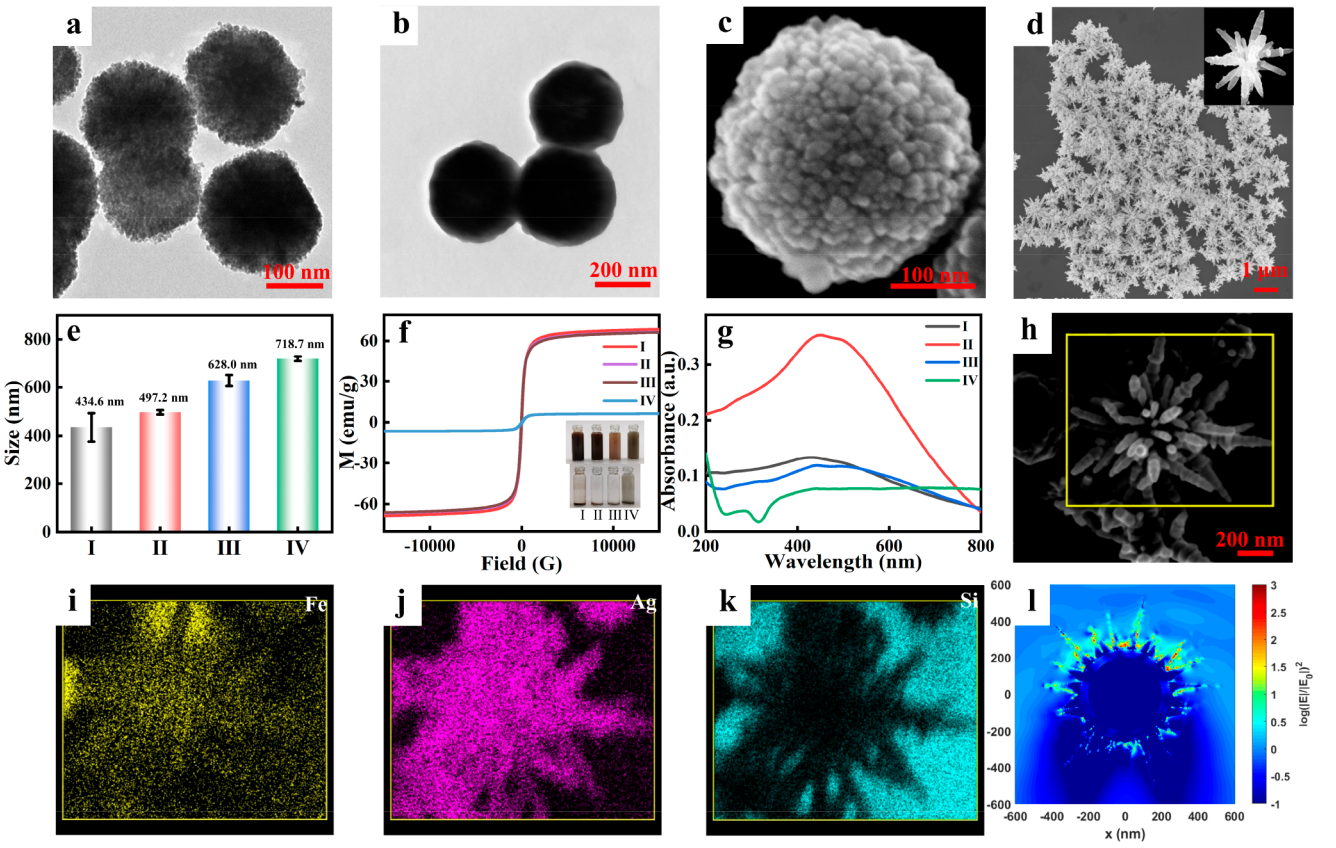

Figure 1. TEM images of Fe_3O_4 (a) and Fe_3O_4@SiO_2 (b), SEM images of Fe_3O_4@SiO_2−Ag seeds (c) and Fe_3O_4@SiO_2@Ag flowers (d); (e) the corresponding hydrated particle size statistical chart; (f) the hysteresis curve chart (inset: the picture before and after magnetic absorption); (g) the UV−vis absorption spectrum; (h−k) the elemental analysis images of Fe_3O_4@SiO_2@Ag flowers; (l) the FDTD simulation diagram of Fe_3O_4@SiO_2@Ag flowers. I−IV are Fe_3O_4, Fe_3O_4@SiO_2, Fe_3O_4@SiO_2−Ag seeds, and Fe_3O_4@SiO_2@Ag flowers, respectively.

applied to analyze FK506 in the blood of transplant patients with high agreement with the clinical results. This sandwich-type probe provides a new potential biosensing technique for the detection of FK506, which is expected to be used for clinical diagnosis.

EXPERIMENTAL SECTION

Material and Reagents. $HAuCl_4{\cdot}3H_2O$, ascorbic acid (AA, 99.7%), and tetraethyl orthosilicate (TEOS) were purchased form Sigma-Aldrich (Beijing, China). $AgNO_3$ (>99.0%), $FeCl_3{\cdot}6H_2O$, ethylene glycol (EG), ethanol, NaOH, N-butylamine, sodium citrate (SC), tannin (TA), $Na_2HPO_4{\cdot}12H_2O$, and NaH_2PO_4 were bought from Sinopharm Group Co., Ltd. (Shanghai, China). *N*-Hydroxysulfosuccinimide (NHS) sodium salt, and N-(3-(dimethylamino)-propyl)-*N*′-ethyl-carbodiimide (EDC) were purchased from Bide Pharmaceutical Technology Co., Ltd. Hexadecyl trimethylammonium bromide (CTAB, 99.0%) and HCHO (37%) were bought from TCI Shanghai (Shanghai, China). Diethylene glycol (DEG) was bought from Sangon Biotech (Shanghai, China). Polyvinylpyrrolidone (PVP, MW = 40000), mycophenolate mofetil, rapamycin, cyclosporine A, and uric acid were bought from Energy Chemical (Shanghai, China). $CH_3COONa{\cdot}3H_2O$, 11-mercaptoundecanoic acid (MUA), bilirubin, and cholesterol were bought from Shanghai Macklin Biochemical Co., Ltd. (Shanghai, China). 5-Amino-2-mercaptobenzimidazole (AMBI) and albumin from bovine serum were bought from Aladdin (Shanghai, China). FK-506 antibody and normal mouse IgM were purchased from Santa Cruz Biotechnology (Shanghai, China). Mouse FK506-binding protein-like (FKBPL) ELISA kit was from Jonin Bio. There was no further purification of any of the chemicals used. All experiments were conducted with deionized water.

Characterization. A TU-1810 UV−vis spectrophotometer (Purkinje General Instrument Co., Ltd., China), HT-7700 transmission electron microscope (Hitachi, Japan), ATR8300-Raman spectrometer (OPTOSKY, China), KQ-600 KDE High Power CNC Ultrasonic Cleaner (Kunshan Shumei, China), Type 7404 Vibrating sample magnetometer (LakeShore, USA), D8 Advance X-ray powder diffractometer (Bruker, Germany), Zeta-sizer nano ZS90 nanoparticle size, and a ζ potential analyzer (Malvern, UK) were used.

Synthesis of Fe_3O_4@SiO_2@Ag Flowers. Fe_3O_4 magnetic particles were synthesized on the basis of ref 37. Afterward, 0.01 g of as-prepared Fe_3O_4 particles was dispersed in a mixture of deionized water-ammonia-ethanol (1 mL/0.8 mL/18 mL). Then, TEOS in ethanol was slowly dropped into the above mixture by vigorously sonicating at room temperature for 60 min. Then, 0.1 g of Fe_3O_4@SiO_2 microspheres was thoroughly cleaned five times with ethanol and then was dispersed in 1 mL ethanol and mixed with 9 mL of $AgNO_3$ (1 mM) for 30 min under vigorous ultrasonication. Subsequently, 5 μL of butylamine (1 M) was added and ultrasonically dispersed for 1 h. The resulting product of Fe_3O_4@SiO_2-Ag seed solution was magnetically separated and dispersed in 20 mL of ethanol for future use. A 0.5 mL aliquot of Fe_3O_4@SiO_2-Ag seed solution was added to 200 mL of 0.2 mM $AgNO_3$ aqueous solution. Then, 150 μL of 37% formaldehyde and 300 μL of 25% ammonia solution were sequentially added. After 2 min, 400 mg of PVP powder was added. The final products of Fe_3O_4@SiO_2@Ag flowers are washed and obtained by magnetic separation.

Synthesis of Ag@Au. The Ag NPs and Ag@Au plasmonic superstructure were prepared according to previous work with slight modification.[21,38] Ag NPs: 100 mL of aqueous solution containing 5 mM SC and TA was heated under vigorous stirring for 15 min. After boiling, 1 mL of 25 mM $AgNO_3$ was injected and then, the solution

https://doi.org/10.1021/acssensors.2c01603
ACS Sens. 2022, 7, 3126−3134

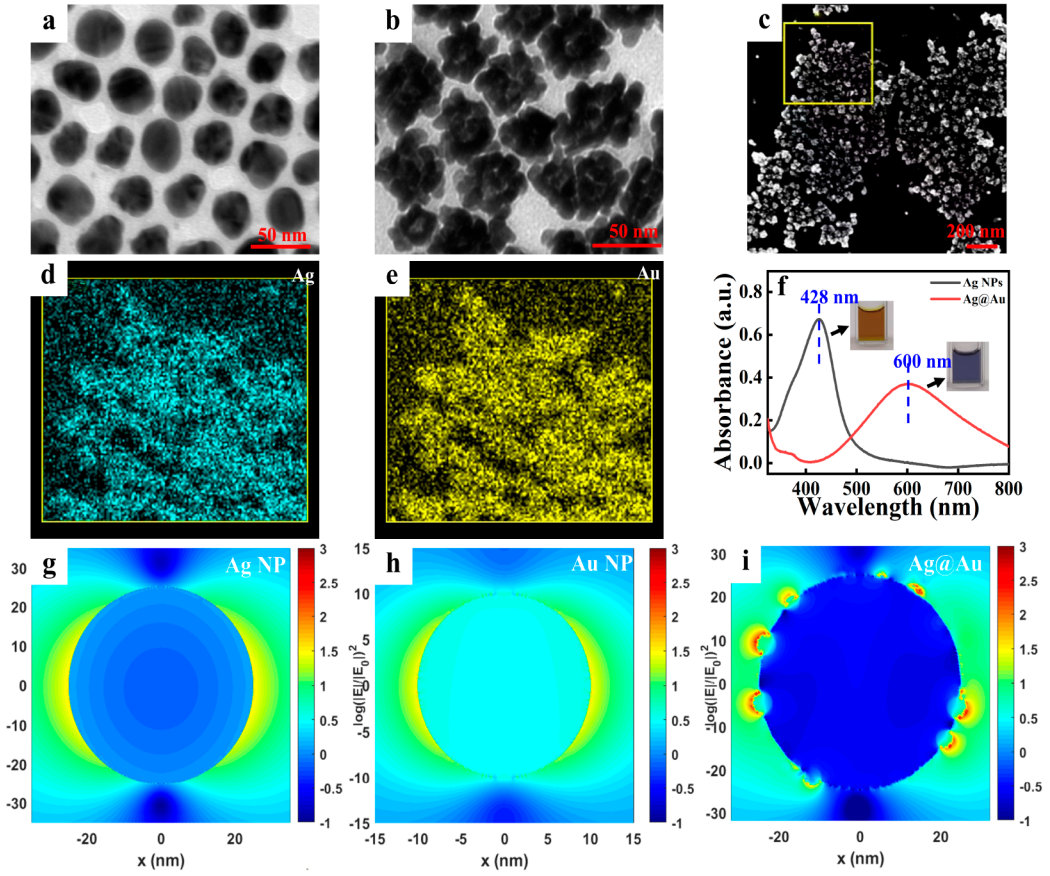

Figure 2. TEM images of Ag NPs (a) and Ag@Au (b); (c–e) SEM images and the elemental analysis images of Ag@Au; (f) the UV–vis absorption spectrum; (g–i) the FDTD simulations of Ag NPs, Au NPs, and Ag@Au.

was cooled. Another 0.5 mL of 25 mM SC and 1.5 mL of 2.5 mM TA were rapidly injected, and then, 1 mL of 25 mM $AgNO_3$ was added after 1 min for reaction. After that, 19.5 mL of sample is discarded, and 16.5 mL of deionized water was added to dilute the seed solution. Under 90 °C, this process was repeated for 4–6 times to obtained the products. The obtained nanoparticles were used by centrifugation and washing.

A 5 mL aliquot of Ag NPs was taken after centrifugation and dispersed in 0.1 M of CTAB. Then, 2.5 mL of 2.5 mM AMBI was added and then diluted to 30 mL under 60 °C for 2 h. Then, 0.1 M of AA, 0.01 M of NaOH, and 0.01 M of $HAuCl_4$ were successively added and diluted to 10 mL under vigorous stirring for 1 min. After standing overnight at 30 °C, the obtained nanoparticles were centrifuged and washed twice with water for further use.

Functionalization of Fe_3O_4@SiO_2@Ag Flowers and Ag@Au with Antibody. Fe_3O_4@SiO_2@Ag flowers-AntiFK506 was adopted by a two-step coupling method. First, the Fe_3O_4@SiO_2@Ag flowers containing 20 mM of MUA were sonicated for 2 h in ethanol solution for carboxylation. Then, 20 mg of NHS and 20 mg of EDC were slowly dripped into the resulting MUA-modified Fe_3O_4@SiO_2@Ag flowers in PBS solution and incubated for 0.5 h at 37 °C. After that, the MUA-modified Fe_3O_4@SiO_2@Ag flowers with surface carboxyl activation were washed by magnetic separation. Lastly, 2 μL of 100 μg/mL of AntiFK506 solution was added and incubated for another 0.5 h, and then, 5% (w/v) of BSA solution was added for another 0.5 h to block the reaction site. The final product was washed and stored in PBS buffer (10 mM, pH 7.4).

IgM was attached onto the surface of Ag@Au through simple Au–S bond action, and the specific experimental process was as follows: 5 μL of 50 μg/mLof IgM was added to 1 mL of Ag@Au solution and incubated for 0.5 h under 37 °C. Similarly, a certain amount of BSA was added the solution to block the reaction site. And the product was also subjected to the same centrifugal washing process and then stored at 4 °C for further use.

Sandwich Immunoassay Protocol for FK506. First, human serum was centrifuged at 1000 rpm for 5 min, and the supernatant was resuspended and diluted 2-fold with PBS solution. A 100 μL aliquot of 0.0125 g/mL of Fe_3O_4@SiO_2@Ag flowers-AntiFK506 was mixed with 1 mL of different serum samples and incubated at 37 °C for 1 h. The resulting complex was collected by magnetic separation and washed with PBS to remove impurities. After that, the Ag@Au-IgM was added into the above solution and incubated for 1 h at 37 °C. Lastly, the resulting sandwich complex was collected by an external magnetic field to wash with PBS for three times and then resuspended in 20 μL of PBS buffer for subsequent SERS measurement. The parameters of the Raman spectrum measurement are set as follows: 633 nm laser, 50× Telephoto objective, 200 mW excitation power, 5000 ms integration time, and a 2 s acquisition time.

Functionalization of Plasmonic Superstructure Fe_3O_4@SiO_2@Ag Flowers and Ag@Au for PSA. The procedure is similar to that of FK506: 100 μL of 0.0125 g/mL of Fe_3O_4@SiO_2@Ag flowers-AntiPSA was mixed with 1 mL of different serum samples and incubated for 1 h at 37 °C. The sample was then washed with PBS and mixed with Ag@Au-AntiPSA for another 1 h at 37 °C. The resulting sandwich complex was collected and washed and resuspended in 20 μL of PBS buffer for subsequent SERS measurement at the same measurement conditions.

RESULTS AND DISCUSSION

Characterization of Fe_3O_4@SiO_2@Ag Flowers. First, Fe_3O_4 nanoparticles with a particle size of 238 ± 12.25 nm, determined by measuring the diameter of about 400 nanoparticles, are synthesized by the solvothermal method (Figure 1a).[37] Then, the Fe_3O_4@SiO_2 and Fe_3O_4@SiO_2-Ag

https://doi.org/10.1021/acssensors.2c01603
ACS Sens. 2022, 7, 3126–3134

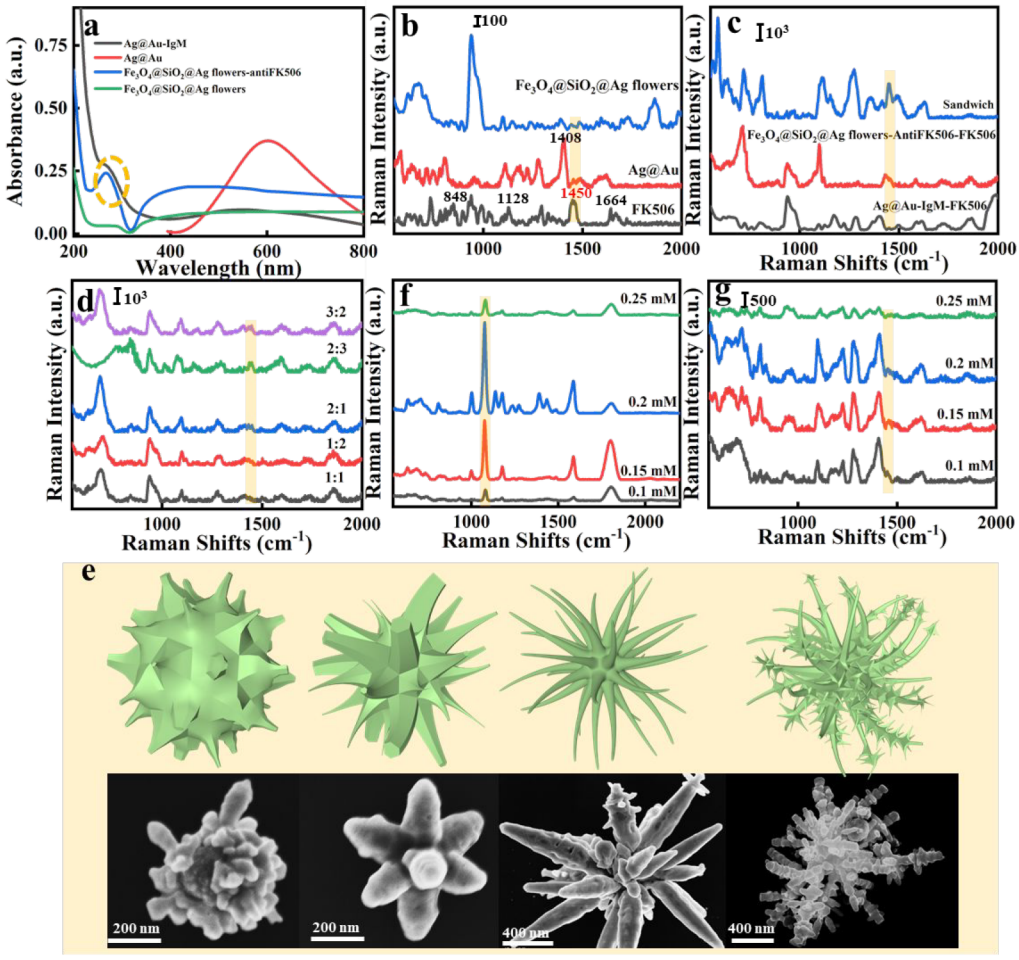

Figure 3. (a) The UV−vis absorption spectrum of different nanoparticles; (b,c) Raman spectrum of different substrates and substances; (d) Raman spectrum of different ratios of Fe_3O_4@SiO_2@Ag flowers-AntiFK506 and Ag@Au-IgM (FK506 = 10 ng/mL); (e) simulated conformation and SEM images of different Fe_3O_4@SiO_2@Ag flowers; (f,g) Raman spectrum of different concentrations of $AgNO_3$ to obtain different Fe_3O_4@SiO_2@Ag flowers for 4-ATP (10^{-4} M) and with Ag@Au-IgM for FK506 (10 ng/mL).

seeds are obtained with particle sizes of about 336 ± 19.7 and 364 ± 13.9 nm, respectively (Figure 1b,c). Finally, the magnetic plasmonic superstructure of Fe_3O_4@SiO_2@Ag flowers with superbranching is successfully prepared. The SEM image clearly indicates that Fe_3O_4@SiO_2@Ag flowers have a flower-like morphology (Figure 1d). And the approximate hydrated particle size is further verified in Figure 1e. The consequent change in zeta potential also further demonstrates the change in surface ligands of the Fe_3O_4@SiO_2@Ag flowers (Figure S1).[40] PVP as a surfactant results in a zeta potential of 28.7 mV for Fe_3O_4. Fe_3O_4@SiO_2 is −37.1 mV for the deprotonation of the hydroxyl group on its surface. In Fe_3O_4@SiO_2-Ag seeds, the zeta potential is −16.0 mV as a result of *n*-butylamine reduction, indicating that oxygen sites are likely to be bound by Ag^+. A further reduction of Fe_3O_4@SiO_2-Ag seeds resulted in Fe_3O_4@SiO_2@Ag flowers (−21.7 mV). And the Fe_3O_4@SiO_2@Ag flowers are further characterized by XRD (Figure S2).[39] Compared with Fe_3O_4, Fe_3O_4@SiO_2, and Fe_3O_4@SiO_2@Ag seeds, the new diffraction peak at 39.4° corresponds to the (111) crystal plane of cubic Ag. When the Ag shell is integrally formed, the new peaks of 39.4° (111), 45.0° (200), and 77.4° (311) prove the successful synthesis of the superstructure. The results of the magnetic response characteristics of the Fe_3O_4@SiO_2@Ag flowers are shown in Figures 1f and S3. The magnetic saturation value gradually decreases with the formation of flower-shaped Ag shells. However, no hysteresis loops are observed for all of the synthesized magnetic particles, indicating that all magnetic particles exhibit superparamagnetic properties. These superparamagnetic properties prevent aggregation and enable rapid redispersal of magnetic nanoparticles in the absence of a magnetic field, thus enabling their application in bioseparation and bioassay. And at the same concentration of different materials can achieve good magnetic separation within the same time (3 min), indicating that the smaller magnetic strength of Fe_3O_4@SiO_2@Ag flowers does not affect the subsequent magnetic separation process for the assay.

Fe_3O_4 typically exhibits resonance absorption around 435 nm with a wider plasma band, which is due to its ferromagnetic behavior, resulting in particle polydispersity. In contrast, when the flower-like Ag shell is formed, a clear resonance absorption peak occurs at 378 nm (Figure 1g).[39] In addition, the elemental analysis further indicates the presence of Fe, O, Si, and Ag and the predominant distribution of Ag in the surface layer (Figure 1h−k). The Ag petals are hundreds of nanometers long with branches on the petals and rich narrow gaps between the particles. These gaps will provide a large number of hot spots for SERS.[34] The FDTD simulation dose

https://doi.org/10.1021/acssensors.2c01603
ACS Sens. 2022, 7, 3126−3134

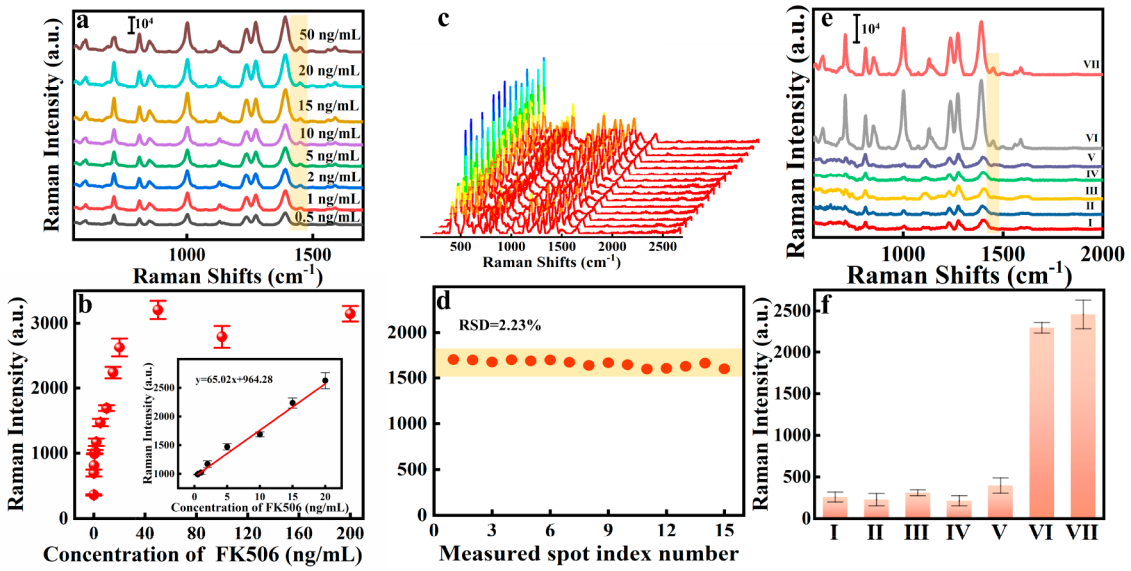

Figure 4. (a,b) The Raman spectrum and linear relationships of the sandwich-type probe for the different concentrations of FK506, respectively. (c,d) The reproducibility of the Raman spectrum and plot figure of sandwich-type probe. (e,f) Raman spectrum and signal statistics at 1450 cm^{-1} of the sandwich-type probe for different analytes (I–VII: bilirubin, cholesterol, rapamycin, mycophenolate, uric acid, and FK506; VII is the mixed sample containing above all).

illustrated in Figure 1l indicates a high intensity electromagnetic field at the silver petal tip.

Characterization of Ag@Au. In SERS, precious metals such as Au and Ag are widely used because of their unique photoelectric properties.[41] Likewise, the bimetallic Ag–Au composite system plays a synergistic role and has better enhanced Raman scattering properties.[42] Consequently, a bimetallic plasmonic superstructure based on Ag@Au is also successfully synthesized. Figure 2a,b shows that the synthesized Ag NPs have good dispersion and size distribution with 38.43 ± 1.4 nm by counting about 200 nanoparticles, and the Ag@Au consists of raspberry-shaped hollow particles with a uniform size of about 59.76 ± 2.8 nm by measuring the average size of 400 nanoparticles. According to the DLS results, the particle size of both Ag NPs and Ag@Au increased relative to TEM due to the influence of hydrated layers (Figure S4a,b). And the zeta potentials of Ag NPs and Ag@Au are −46.0 and 53.5 mV, respectively, for the presence of carboxyl ligands and CTAB on the surfaces (Figure S4c). The elemental distribution in SEM (Figure 2c–e) and XRD (Figure S5) also proved the successful synthesis of the Ag@Au bimetallic plasmonic superstructure. In addition, a change in UV–vis in Figure 2f further indicates that the acquisition of Ag@Au bimetallic plasmonic superstructure has been successful, as the absorption peak shifts from 428 nm (Ag NPs) to the 600 nm (Ag@Au), which is primarily due to the plasmon resonance absorption of Au. According to FDTD simulations, both silver nanospheres and gold nanospheres exhibit lower electromagnetic field strengths than Ag@Au bimetallic composite plasma superstructures (Figure 2g–i). SERS signals may be improved by designing superstructures based on the theoretical results presented.

Optimized Condition for Sensing FK506. For the purpose of constructing a SERS biosensor for detecting FK506 with good specificity and high sensitivity by Fe_3O_4@SiO_2@Ag flowers and Ag@Au, Fe_3O_4@SiO_2@Ag flowers and Ag@Au are further modified using FK506 specific antibodies (antiFK506) and IgM antibodies, respectively. As shown in Figure 3a, the UV absorption profiles of Fe_3O_4@SiO_2@Ag flowers and Ag@Au modified antibodies both have distinct protein characteristic absorption peaks around 280 nm. The packaging efficiency of AntiFK506 on is 68.98% (Figure S6). And the corresponding characterization of zeta, DLS, and stability is shown in Figures S7–S9. Fe_3O_4@SiO_2@Ag flowers are modified with MUA prior to modification of antiFK506 owing to the sulfhydryl group at the one end of MUA, which can form a Ag–S bond, while the carboxyl group at the other end can be used to combine with the amino group on the FK506 antibody by forming an amide bond. So, after connecting MUA and antiFK506, Fe_3O_4@SiO_2@Ag flowers' particle size gradually increased (Figure S7a,b), and the zeta potential changed from −21.7 to −22.4 and then to −10.0 mV (Figure S7c). This phenomenon should be caused by the carboxyl group at one end of MUA, resulting in a more negative potential. A significant increase in zeta potential is observed when antiFK506 is modified to form a film on the surfaces of strongly negative Ag shells. The particle size increased to 165.5 nm after Ag@Au is coupled with the IgM antibody, and the zeta potential increased significantly (Figure S8). It was also demonstrated that the two superstructures of modified antibody could be stabilized without changing their properties for over five months, as evidenced by their performance in detection experiments (Figure S9).

Then, as shown in Figure 3b, the Raman signal of Fe_3O_4@SiO_2@Ag flowers, Ag@Au, and FK506 showed FK506 with several Raman peaks including 848 cm^{-1} (bending out of plane of C–H, C–O–C, and C–C–C), 1128 cm^{-1} (bending in-plane of aromatic ring), 1450 cm^{-1} (C–OH stretching), and 1664 cm^{-1} ($H_2C{=}CH_2$ stretching).[43] There was a characteristic peak at 1408 cm^{-1} in the interface energy controlled by the AMBI ligand Ag@Au,[43−45] In contrast, Fe_3O_4@SiO_2@Ag flowers did not show any obvious characteristic absorption peak. Consequently, the Raman characteristic peak of FK506 at 1450 cm^{-1} is selected for subsequent quantitative experimental analysis. And the sandwich-type probe-enhanced FK506 Raman signal is 5–10 times stronger than that of the

https://doi.org/10.1021/acssensors.2c01603
ACS Sens. 2022, 7, 3126−3134

single plasmonic superstructure (Figure 3c). This result also tentatively demonstrates that the sandwich-type probe has a significant effect on the enhancement of Raman signal. In addition, the SEM image clearly demonstrated that the sandwich superstructure of Fe_3O_4@SiO_2@Ag flowers-AntiFK506-FK506-IgM-Ag@Au had been successfully formed (Figure S10).

The enhancement effect of the sandwich-type probe for FK506 was investigated. As shown in Figures 3d and S11, the Raman signal is best when the ratio of Fe_3O_4@SiO_2@Ag flowers-AntiFK506 to Ag@Au-IgM is 3:2. And as shown in Figure 3e, the number and length of petals of the magnetic Ag flower increased with the gradual increase of $AgNO_3$ concentration. Fe_3O_4@SiO_2@Ag flowers exhibit the best enhancement effect on 4-ATP when the $AgNO_3$ concentration is 0.25 mM (Figure 3f). And the same excellent results are obtained in the detection of FK506 with Fe_3O_4@SiO_2@Ag flowers (Figure 3g). The main reason for this is that too many Ag flower petals reduce the stacking density of magnetic Ag flowers, which adversely affects the formation of interparticle hot spots. At the same time, Ag flake petals that are too long and too many branches reduce the dispersion and magnetic responsiveness of Ag flake particles.

Detection of FK506 in Complex Sample and Patient's Blood. After optimizing various conditions, FK506 was quantified using a sandwich-type probe. As shown in Figure 4a,b, the SERS signal peak at 1450 cm^{-1} increased continuously in the concentration range of 0.01−200 ng/mL of FK506. The linearity is good in the range of 0.5−20 ng/mL ($y = 65.02x + 964.28$), and the detection limit is 0.33 ng/mL. Compared with other methods, it has better advantages in detection limit and sensitivity (Table S1). As shown in Figure 4c,d, the RSD of Raman detection for 15 randomly selected measurement points on the substrate is 2.23%, indicating the good homogeneity of the SERS probe. The sandwich-type probe is capable of detecting FK506 quantitatively with a high degree of specificity. The presence of other macrolide immunosuppressants, coapplied drugs, and interfering substances in the serum environment does not produce any distinctive characteristic signal at 1450 cm^{-1} (Figures 4e,f and S12). And the recoveries of FK506 in PBS buffer and human serum are further examined to detect FK506 in complex systems by a sandwich-type probe. As shown in Figure S13 and Table S2, the recoveries are 96.7−102.9% in PBS buffer and 98.0−103.0% in human serum, respectively. These results indicate that the sandwich-type probe has the ability to specifically detect FK506 in a complex environment.

As a result, two gland transplant and three renal transplant patients were analyzed using the sandwich-type probe for FK506 in serum samples (Figure 5a). FK506 was successfully detected in blood samples, which demonstrates the reliability of the sandwich-type probe in real samples and shows the promise for the immunoassay in clinical organ transplant patients. In addition, the calibration results were basically consistent with those of commercial kits, which further proves the accuracy of the platform (Figure 5b,c). And replacement of surface ligands of the Fe_3O_4@SiO_2@Ag flower and Ag@Au plasmonic superstructure enable the detection of other biomarkers (Figure S14). Those findings demonstrate that the Fe_3O_4@SiO_2@Ag flower and Ag@Au plasmonic superstructures are universal in the detection of biomarkers and indirectly suggest that the sandwich-type probe SERS platform is of considerable practical value.

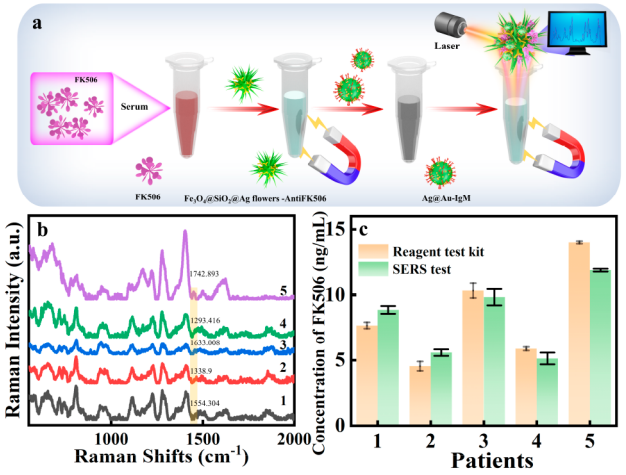

Figure 5. (a) Scheme of FK506 detection in patient blood samples; (b,c) Raman spectrograms and signal statistics of FK506 detection in patient blood samples.

CONCLUSIONS

In all, a simple and effective method for detecting FK506 in blood has been developed by double plasmonic superstructures (Fe_3O_4@SiO_2@Ag flowers and Ag@Au). The sandwich plasmonic superstructure SERS platform for the detection of FK506 was demonstrated with high sensitivity, specificity, and reproducibility. The detection limit of FK506 is 0.33 ng/mL with a detection window of 5−20 ng/mL. Moreover, this method can also be capable of monitoring the level of FK506 in the serum of actual patients. Furthermore, the plasmonic superstructures can be utilized for the analysis and detection of other disease markers. Therefore, the proposed sandwich-type SERS biosensor is a simple and attractive technique for real sample detection, which has the potential to be used for the clinical diagnosis.

ASSOCIATED CONTENT

Supporting Information

The Supporting Information is available free of charge at https://pubs.acs.org/doi/10.1021/acssensors.2c01603.

DLS, zeta potential, and XRD characterization of different magnetic materials and Ag@Au, magnetic statistics and stability of different magnetic materials, Raman performance test of the superstructure, table of recovery tests for FK506 in spiked PBS buffer and human serum samples, standard curve of FK506 by an ELISA kit (PDF)

AUTHOR INFORMATION

Corresponding Authors

Caiping Ding − *College of Material, Chemistry and Chemical Engineering, Key Laboratory of Organosilicon Chemistry and Material Technology, Ministry of Education, Hangzhou Normal University, Hangzhou 311121 Zhejiang, China*; Email: cpding@hznu.edu.cn

Youju Huang − *College of Material, Chemistry and Chemical Engineering, Key Laboratory of Organosilicon Chemistry and Material Technology, Ministry of Education, Hangzhou Normal University, Hangzhou 311121 Zhejiang, China*; orcid.org/0000-0001-5815-9784; Email: yjhuang@hznu.edu.cn

https://doi.org/10.1021/acssensors.2c01603
ACS Sens. 2022, 7, 3126−3134

Authors

Xiaoyue Zheng − *College of Material, Chemistry and Chemical Engineering, Key Laboratory of Organosilicon Chemistry and Material Technology, Ministry of Education, Hangzhou Normal University, Hangzhou 311121 Zhejiang, China*

Jiazhou Ye − *College of Material, Chemistry and Chemical Engineering, Key Laboratory of Organosilicon Chemistry and Material Technology, Ministry of Education, Hangzhou Normal University, Hangzhou 311121 Zhejiang, China*

Weiwei Chen − *College of Material, Chemistry and Chemical Engineering, Key Laboratory of Organosilicon Chemistry and Material Technology, Ministry of Education, Hangzhou Normal University, Hangzhou 311121 Zhejiang, China*

Xiaoyuan Wang − *College of Material, Chemistry and Chemical Engineering, Key Laboratory of Organosilicon Chemistry and Material Technology, Ministry of Education, Hangzhou Normal University, Hangzhou 311121 Zhejiang, China*

Jianhua Li − *Anhui Topway Testing Services Co., Ltd., Anhui 242000, China*

Fengmei Su − *National Engineering Research Centre for Advanced Polymer Processing Technology, Zhengzhou University, Zhengzhou 450002, China;* orcid.org/0000-0002-7124-0269

Complete contact information is available at: https://pubs.acs.org/10.1021/acssensors.2c01603

Author Contributions

C.D. and Y.H. contributed equally.

Notes

The authors declare no competing financial interest.

■ ACKNOWLEDGMENTS

This work was financially supported in part by the National Natural Science Foundation of China (Grant Nos. 22005081, 52111530128, and 52222316), the Zhejiang Provincial Natural Science Foundation of China (LY22B050003 and LZ22B050001), and the Key Research and Development Projects of Anhui Province (202104g01020009).

■ REFERENCES

(1) Scott, L. J; McKeage, K.; Keam, S. J; Plosker, G. L Tacrolimus: a further update of its use in the management of organ transplantation. *Drugs* **2003**, *63*, 1247−1297.

(2) Kamel, M.; Kadian, M.; Srinivas, T.; Taber, D.; Salas, M. A. P. Tacrolimus confers lower acute rejection rates and better renal allograft survival compared to cyclosporine. *World J. Transplant.* **2016**, *6*, 697−702.

(3) Peters, D. H.; Fitton, A.; Plosker, G. L.; Faulds, D. Tacrolimus. A review of its pharmacology, and therapeutic potential in hepatic and renal transplantation. *Drugs* **1993**, *46*, 746−794.

(4) Murakami, Y.; Endo, T.; Yamamura, S.; Nagatani, N.; Takamura, Y.; Tamiya, E. On-chip micro-flow polystyrene bead-based immunoassay for quantitative detection of tacrolimus (FK506). *Anal. Biochem.* **2004**, *334*, 111−116.

(5) Salis, F.; Descalzo, A. B.; Benito-Peña, E.; Moreno-Bondi, M. C.; Orellana, G. Highly fluorescent magnetic nanobeads with a remarkable stokes shift as labels for enhanced detection in immunoassays. *Small* **2018**, *14*, No. 1703810.

(6) Wu, J.; Zheng, Z.; Chong, Y.; Li, X.; Pu, L.; Tang, Q.; Yang, L.; Wang, X.; Wang, F.; Liang, G. Immune responsive release of tacrolimus to overcome organ transplant rejection. *Adv. Mater.* **2018**, *30*, No. 1805018.

(7) Kalt, D. A. Tacrolimus: a review of laboratory detection methods and indications for use. *Lab. Med.* **2017**, *48*, No. e62.

(8) Brunet, M.; Gelder, T. V.; Bergan, S.; et al. Therapeutic drug monitoring of tacrolimus-personalized therapy: second consensus report. *Ther. Drug Monit.* **2019**, *41*, 261−307.

(9) Cangemi, G.; Barco, S.; Bonifazio, P.; Maffia, A.; Agazzi, A.; Melioli, G. Comparison of antibody-conjugated magnetic immunoassay and liquid chromatography-tandem mass spectrometry for the measurement of cyclosporine and tacrolimus in whole blood. *Int. J. Immunopathol. Pharmacol.* **2013**, *26*, 419−426.

(10) Ju, M.K.; Chang, H.K.; Kim, H.J.; Huh, K.H.; Ahn, H.J.; Kim, M.S.; Kim, S.I.; Kim, Y.S. Is the affinity column-mediated immunoassay method suitable as an alternative to the microparticle enzyme immunoassay method as a blood tacrolimus assay? *Transplant. Proc.* **2008**, *40*, 3673−3678.

(11) Kim, H. K.; Park, H. D.; Lee, S. G.; Chae, H.; Song, S. H.; Lee, Y. W.; Yun, Y. M.; Ahn, S.; Kim, S.; Lee, S. M.; Lee, S. Y.; Chun, S. Immunosuppressive drug measurement by liquid chromatography coupled to tandem mass spectrometry: Interlaboratory comparison in the Korean clinical laboratories. *Ann. Lab. Med.* **2021**, *41*, 268−276.

(12) Becker, S.; Thiery, J.; Ceglarek, U. Evaluation of a novel commercial assay for the determination of cyclosporine A, tacrolimus, sirolimus, and everolimus by liquid chromatography-tandem mass spectrometric assay. *Ther. Drug Monit.* **2013**, *35*, 129−132.

(13) Fleischmann, M.; Hendra, P. J.; McQuillan, A. J. Raman spectra of pyridine adsorbed at a silver electrode. *Chem. Phys. Lett.* **1974**, *26*, 163−166.

(14) Cardinal, M. F.; Vander Ende, E.; Hackler, R. A.; McAnally, M. O.; Stair, P. C.; Schatz, G. C.; Van Duyne, R. P. Expanding applications of SERS through versatile nanomaterials engineering. *Chem. Soc. Rev.* **2017**, *46*, 3886−3903.

(15) Langer, J.; Aberasturi, D. J. D.; Liz-Marzán, L. M.; et al. Present and future of surface-enhanced Raman scattering. *ACS Nano* **2020**, *14*, 28−117.

(16) Guselnikova, O.; Lim, H.; Na, J.; Eguchi, M.; Kim, H.-J.; Elashnikov, R.; Postnikov, P.; Svorcik, V.; Semyonov, O.; Miliutina, E.; Lyutakov, O.; Yamauchi, Y. Enantioselective SERS sensing of pseudoephedrine in blood plasma biomatrix by hierarchical mesoporous Au films coated with a homochiral MOF. *Biosens. Bioelectron.* **2021**, *180*, 113109.

(17) Hang, Y.; Boryczka, J.; Wu, N. Visible-light and near-infrared fluorescence and surface-enhanced Raman scattering point-of-care sensing and bio-imaging: a review. *Chem. Soc. Rev.* **2022**, *51*, 329−375.

(18) Song, L.; Chen, J.; Xu, B. B.; Huang, Y. Flexible plasmonic biosensors for healthcare monitoring: progress and prospects. *ACS Nano* **2021**, *15*, 18822−18847.

(19) Song, L.; Xu, B. B.; Cheng, Q.; Wang, X.; Luo, X.; Chen, X.; Chen, T.; Huang, Y. Instant interfacial self-assembly for homogeneous nanoparticle monolayer enabled conformal ″lift-on″ thin film technology. *Sci. Adv.* **2021**, *7*, No. eabk2852.

(20) Tian, T.; Yi, J.; Liu, Y.; Li, B.; Liu, Y.; Qiao, L.; Zhang, K.; Liu, B. Self-assembled plasmonic nanoarrays for enhanced bacterial identification and discrimination. *Biosens. Bioelectron.* **2022**, *197*, 113778.

(21) Shao, H.; Lin, H.; Guo, Z.; Lu, J.; Jia, Y.; Ye, M.; Su, F.; Niu, L.; Kang, W.; Wang, S.; Hu, Y.; Huang, Y. A multiple signal amplification sandwich-type SERS biosensor for femtomolar detection of miRNA. *Biosens. Bioelectron.* **2019**, *143*, 111616.

(22) Singha, S. S.; Mondal, S.; Bhattacharya, T. S.; Das, L.; Sen, K.; Satpati, B.; Das, K.; Singha, A. Au nanoparticles functionalized 3D-MoS_2 nanoflower: An efficient SERS matrix for biomolecule sensing. *Biosens. Bioelectron.* **2018**, *119*, 10−17.

(23) Huang, Y.; Dai, L.; Song, L.; Zhang, L.; Rong, Y.; Zhang, J.; Nie, Z.; Chen, T. Engineering gold nanoparticles in compass shape with broadly tunable plasmon resonances and high-performance SERS. *ACS Appl. Mater. Interfaces* **2016**, *8*, 27949−27955.

(24) Huang, Y.; Ferhan, A. R.; Cho, S. J.; Lee, H.; Kim, D.-H. Gold nanowire bundles grown radially outward from silicon micropillars. *ACS Appl. Mater. Interfaces* **2015**, *7*, 17582−17586.
(25) Chen, J.; Huang, Y.; Kannan, P.; Zhang, L.; Lin, Z.; Zhang, J.; Chen, T.; Guo, L. Flexible and adhesive surface enhance Raman scattering active tape for rapid detection of pesticide residues in fruits and vegetables. *Anal. Chem.* **2016**, *88*, 2149−2155.
(26) Guo, Z.; Jia, Y.; Song, X.; Lu, J.; Lu, X.; Liu, B.; Han, J.; Huang, Y.; Zhang, J.; Chen, T. Giant gold nanowire vesicle-based colorimetric and SERS dual-mode immunosensor for ultrasensitive detection of Vibrio parahemolyticus. *Anal. Chem.* **2018**, *90*, 6124−6130.
(27) Lu, X.; Huang, Y.; Liu, B.; Zhang, L.; Song, L.; Zhang, J.; Zhang, A.; Chen, T. Light-controlled shrinkage of large-area gold nanoparticle monolayer film for tunable SERS activity. *Chem. Mater.* **2018**, *30*, 1989−1997.
(28) Song, L.; Huang, Y.; Nie, Z.; Chen, T. Macroscopic two-dimensional monolayer films of gold nanoparticles: fabrication strategies, surface engineering and functional applications. *Nanoscale* **2020**, *12*, 7433−7460.
(29) Gao, Q.; Zhao, A.; Gan, Z.; Tao, W.; Li, D.; Zhang, M.; Guo, H.; Wang, D.; Sun, H.; Mao, R.; Liu, E. Facile fabrication and growth mechanism of 3D flower-like Fe_3O_4 nanostructures and their application as SERS substrates. *CrystEngComm* **2012**, *14*, 4834−4842.
(30) Xu, Y.; Hassan, M. M.; Zhu, A.; Li, H.; Chen, Q. Dual-mode of magnetic assisted Au@Ag SERS tags and cationic conjugated UCNPs for qualitative and quantitative analysis of multiple foodborne pathogens. *Sens. Actuators B: Chem.* **2021**, *344*, 130305.
(31) Hong, X.; Chu, X.; Zou, P.; Liu, Y.; Yang, G. Magnetic-field-assisted rapid ultrasensitive immunoassays using Fe_3O_4/ZnO/Au nanorices as Raman probes. *Biosens. Bioelectron.* **2010**, *26*, 918−922.
(32) Zhu, R.; Feng, H.; Li, Q.; Su, L.; Fu, Q.; Li, J.; Song, J.; Yang, H. Asymmetric core-shell gold nanoparticles and controllable assemblies for SERS ratiometric detection of microRNA. *Angew. Chem., Int. Ed.* **2021**, *60*, 12560−12568.
(33) Liang, H.; Li, Z.; Wang, W.; Wu, Y.; Xu, H. Highly surface-roughened "flower-like" silver nanoparticles for extremely sensitive substrates of surface-enhanced Raman scattering. *Adv. Mater.* **2009**, *21*, 4614−4618.
(34) Wang, C.; Wang, J.; Li, P.; Rong, Z.; Jia, X.; Ma, Q.; Xiao, R.; Wang, S. Sonochemical synthesis of highly branched flower-like Fe_3O_4@SiO_2@Ag microcomposites and their application as versatile SERS substrates. *Nanoscale* **2016**, *8*, 19816−19828.
(35) Li, J. F.; Zhang, Y. J.; Ding, S. Y.; Panneerselvam, R.; Tian, Z. Q. Core-shell nanoparticle-enhanced Raman spectroscopy. *Chem. Rev.* **2017**, *117*, 5002−5069.
(36) Guo, J.; Yan, X.; Xu, M.; Ghimire, G.; Pan, X.; He, J. Effective electrochemical modulation of SERS intensity assisted by core-shell nanoparticles. *Anal. Chem.* **2021**, *93*, 4441−4448.
(37) Xuan, S.; Wang, F.; Wang, Y. X. J.; Yu, J. C.; Leung, K. C. F. Facile synthesis of size-controllable monodispersed ferrite nanospheres. *J. Mater. Chem.* **2010**, *20*, 5086−5094.
(38) Jin, L.; Shen, S.; Huang, Y.; Li, D.; Yang, X. Corn-like Au/Ag nanorod-mediated NIR-II photothermal/photodynamic therapy potentiates immune checkpoint antibody efficacy by reprogramming the cold tumor microenvironment. *Biomaterials* **2021**, *268*, 120582.
(39) Wang, C.; Rong, Z.; Wang, J.; Jiang, N.; Pang, Y.; Xiao, R.; Wang, S. Seed-mediated synthesis of high-performance silver-coated magnetic nanoparticles and their use as effective SERS substrates. *Colloids and Surf. A Physicochem. Eng. Aspects* **2016**, *506*, 393−401.
(40) Kyrychenko, A.; Korsun, O. M.; Gubin, I. I.; Kovalenko, S. M.; Kalugin, O. N. Atomistic simulations of coating of silver nanoparticles with poly(vinylpyrrolidone) oligomers: effect of oligomer chain length. *J. Phys. Chem. C* **2015**, *119*, 7888−7899.
(41) Kang, H.; Buchman, J. T.; Rodriguez, R. S.; Ring, H. L.; He, J.; Bantz, K. C.; Haynes, C. L. Stabilization of silver and gold nanoparticles: preservation and improvement of plasmonic functionalities. *Chem. Rev.* **2019**, *119*, 664−699.
(42) Ha, M.; Kim, J. H.; You, M.; Li, Q.; Fan, C.; Nam, J.-M. Multicomponent plasmonic nanoparticles: from heterostructured nanoparticles to colloidal composite nanostructures. *Chem. Rev.* **2019**, *119*, 12208−12278.
(43) Camargo, G. d. A.; Costa Filha, A. R. C. d.; Lyra, A. M.; Novatski, A.; Nadal, J. M.; de Lara, L. S.; Dias, D. T.; Nascimento, E. A. d.; Rocha Silva, U.; Jacinto, C.; Farago, P. V. Stability testing of tacrolimus-loaded poly(ε-caprolactone) nanoparticles by physicochemical assays and Raman spectroscopy. *Vib. Spectrosc.* **2020**, *110*, 103139.
(44) Chen, Y.; Yang, J.; Li, Z.; Li, R.; Ruan, W.; Zhuang, Z.; Zhao, B. Experimental and density functional theory study of Raman and SERS spectra of 5-amino-2-mercaptobenzimidazole. *Spectrochim. Acta. A Mol. Biomol. Spectrosc.* **2016**, *153*, 344−348.
(45) Jorio, A.; Souza Filho, A. G. Raman studies of carbon nanostructures. *Annu. Rev. Mater. Res.* **2016**, *46*, 357−382.

https://doi.org/10.1021/acssensors.2c01603
ACS Sens. 2022, 7, 3126−3134